



Article

Pixel-Based Long-Term (2001–2020) Estimations of Forest Fire Emissions over the Himalaya

Somnath Bar ¹, Bikash Ranjan Parida ¹, Arvind Chandra Pandey ¹ and Navneet Kumar ^{2,*}

¹ Department of Geoinformatics, School of Natural Resource Management, Central University of Jharkhand, Ranchi 835222, India

² Department of Ecology and Natural Resources Management, Center for Development Research (ZEF), University of Bonn, 53113 Bonn, Germany

* Correspondence: nkumar@uni-bonn.de

Abstract: Forest/wildfires have been one of the most notable severe catastrophes in recent decades across the globe, and their intensity is expected to rise with global warming. Forest fire contributes significantly to particulate and gaseous pollution in the atmosphere. This study has estimated the pixel-based emissions (CO, CO₂, CH₄, NO_x, SO₂, NH₃, PM_{2.5}, PM₁₀, OC, and BC) from forest fires over the Himalaya (including India, Nepal, and Bhutan). The MODIS-based burned area (MCD64A1), Land Use Land Cover (LULC; MCD12A1), NDVI (MOD13A2), percentage tree cover (MOD44A6), gridded biomass, and species-wise emissions factors were used to estimate the monthly emissions from forest fires over the last two decades (2001–2020). A bottom-up approach was adopted to retrieve the emissions. A substantial inter-annual variation of forest burn area was found over the western, central (Nepal), and eastern Himalaya (including Bhutan). The eastern Himalaya exhibited the highest average annual CO₂ emission, i.e., 20.37 Tg, followed by Nepal, 15.52 Tg, and the western Himalaya, 4.92 Tg. Spatially, the higher CO₂ (0.01–0.02 Tg year⁻¹/km²) and CO (0.007–0.002 Tg year⁻¹/km²) emissions were detected along the south-eastern parts of the eastern Himalaya, southern regions of Nepal, and south-eastern parts of the western Himalaya. The trend of forest fire emissions in 2001–2010 was significantly positive, while in the next decade (2011–2020) a negative trend was recorded. The estimated pixel-based emission and Global Fire Emission Dataset (GFEDv4.1s) data demonstrated a promising association with a correlation coefficient (*r*) between 0.80 and 0.93. An inventory of forest fire emissions over long-term periods can be helpful for policymakers. In addition, it helps to set guidelines for air quality and atmospheric transport modelling and to better understand atmospheric pollution over the Himalayan and associated regions.



Citation: Bar, S.; Parida, B.R.; Pandey, A.C.; Kumar, N. Pixel-Based Long-Term (2001–2020) Estimations of Forest Fire Emissions over the Himalaya. *Remote Sens.* **2022**, *14*, 5302. <https://doi.org/10.3390/rs14215302>

Academic Editor: Melanie Vanderhoof

Received: 23 August 2022

Accepted: 20 October 2022

Published: 23 October 2022

Publisher's Note: MDPI stays neutral with regard to jurisdictional claims in published maps and institutional affiliations.



Copyright: © 2022 by the authors. Licensee MDPI, Basel, Switzerland. This article is an open access article distributed under the terms and conditions of the Creative Commons Attribution (CC BY) license (<https://creativecommons.org/licenses/by/4.0/>).

Keywords: forest fire; burn area; emissions; spatio-temporal variation; MODIS; Himalaya

1. Introduction

Open biomass burning (including forest and grass and crop fires) release significant amounts of greenhouse gases (CO₂ and CH₄), trace gases (CO, NO_x, SO₂, NH₃, etc.), and particulate matter (PM₁₀ and PM_{2.5}) that play an important role in atmospheric chemistry [1–3]. Biomass burning is the largest source of black carbon (BC) and accounts for 59% of BC emissions, 85% of primary organic aerosol (POA) [4], and 40% of carbon dioxide (CO₂) worldwide [5,6]. Open biomass burning contributes one-third to one-half of worldwide carbon monoxide (CO) and 20% of nitrogen oxide (NO_x) emissions [7]. Furthermore, fires release more than 100 million tonnes of smoke aerosol into the atmosphere every year, with tropical fires accounting for about 80% of total smoke aerosol emissions [8]. Moreover, forest fire is one of the largest contributors of mercury emission to the atmosphere, and the average annual mercury emission over the tropical continents is 497 Mg (ranging between 289 to 681 Mg) [9]. These emissions (gaseous and particulate matter) from forest/wildfires have significantly altered the chemical compositions of the lower atmosphere

and deteriorated regional and global air quality, and they have substantial adverse effects on human health, ecosystem productivity, and environmental health [10–14]. According to studies, the annual mortality due to outdoor air pollution is 4.2 million (ranging from 3.7 to 4.8 million with 95% uncertainties), and open vegetation fire smoke accounts for up to 0.6 million premature deaths worldwide [15–17]. The emitted greenhouse gases, trace gases, and particulate matter from forest fires, and their long-range transport, have contributed significantly to regional and global warming and climate change [2,18]. Conversely, the changing climate (longer dry spells and higher temperatures) has significantly increased the severity of forest fires and also altered the spatiotemporal dynamics of fire regimes (i.e., fire size, season, pattern, and frequency) [19–21]. Human-induced forest/wildfire episodes and their emissions also affect ecosystem functionality and biodiversity [14,22]. Forest fire, including shrubland and grassland fire emissions, is an important input parameter and a significant source of uncertainty in air pollutant transport modelling and terrestrial biogeochemical modelling [23,24]. Thus, a precise estimate of forest fire emissions is required to minimize uncertainty in atmospheric and terrestrial models and reveal their contribution to air pollution and climate change [25].

The estimation of forest/wildfire emissions is mainly based on the bottom-up and top-down approaches [3]. The bottom-up approach has been extensively used to investigate forest fire emissions by plant functional types, including studies of near real-time PM_{2.5} emissions over the US, mercury emissions over the tropical continents [9], and emissions from forest and crop fires over China [25] and India [22,26]. The bottom-up technique is based on the amount and type of aboveground biomass burnt as a function of time, space, combustion efficiency, and species-wise emission factor, which is the amount of emission of a specific species per unit of biomass burned [3,27]. Fuel load/biomass data are available at the regional scale, derived using explicit satellite measurements and extensive field observations, and serve as a reliable source for quantifying forest fire emissions [28]. The combustion efficiency/factor is an essential factor that defines the spatiotemporal variations of the fuel moisture condition. However, studies have used the vegetation condition index (VCI) to quantify the combustion factor across tree cover fractions (T_c), i.e., >60% forest, 40–60% shrubland, and 40% grassland [9,25]. Fire radiative energy (FRE), the rate of radiative energy during the combustion processes, can also be used to estimate emissions from open biomass burning [29,30]. The FRE-based method can reduce uncertainty in satellite-derived burn area data, particularly for smaller and short-lived fires [25,31–33]. However, the main shortcoming of this method is the temporal revisiting interval of the satellite overpass. A frequent satellite observation (e.g., 15 min for Meteosat second generation) is essential to track proper fire dynamics for a more accurate assessment of biomass burning emissions from FRE [34]. However, this type of satellite observation is limited. The top-down approach is based on downscaling the available atmospheric pollutants to predict emissions from open biomass burning. However, this method has a considerable approximation, dependent on the accuracy of measured atmospheric pollutants and the other sources of the pollutants over the region [35,36]. The bottom-up (based on the burned area approach) technique has become more significant in estimating open biomass burning emissions globally.

The Himalayan forest belt is one of the most fragile ecosystems; uncontrolled forest fire is a frequent phenomenon, which is the main reason for forest degradation, diminishing ecosystem productivity, and biodiversity losses [22,37–39]. Forest fires in the Himalaya have been linked to poor air quality in non-monsoon seasons [40–42]. The studies revealed a significant deposition of BC from biomass burning over Himalayan glaciers such as Gangotri and Tapovan during the peak fire season [43–45]. BC is a climate-forcing agent that could enhance the rate of ice melting by lowering visible albedo, i.e., 4.2–5.1% [46]. Northern Indian biomass burning in the springtime has a significant cooling effect of -27 W m^2 and -8 W m^2 at the surface and top of the atmosphere, respectively, over lower polluted high altitudes in the central Himalaya [47]. Changes caused by biomass burning emissions may lead to greater absorption of short waves above the cloud, potentially

altering monsoon rainfall [47]. Because of higher forest fire activity in 2016, BC and organic carbon (OC) emissions heat up the Himalayan atmosphere at a rate of $0.04\text{--}0.06\text{ K day}^{-1}$, and changes in metrological conditions and BC contribute to a 5–20% drop in the fraction of snow cover [48]. With the help of long-rage transport, forest fire emissions could significantly affect the surrounding region's environment. For this reason, a comprehensive and consistent measurement of forest fire emissions is important to early monitor and predict pollutants-induced changes in the surrounding regions.

Remote sensing-based measurements and geospatial tools have broadened the scope of open biomass burning monitoring and assessment across the globe [49–52]. Through the extensive use of remote sensing measures, burn area identification, biomass estimation, and combustion completeness computation have been possible. Himalayan forest fire activities have a long historical legacy, but a continuous monitoring of fire emissions in a higher resolution is limited. The present study has addressed this gap and examined emissions with respect to metrological conditions. The specific objectives of this study are to (i) develop a long-term (2001–2020) and high-resolution ($1\text{ km} \times 1\text{ km}$) emissions inventory (i.e., CO , CO_2 , CH_4 , NO_x , SO_2 , NH_3 , $\text{PM}_{2.5}$, PM_{10} , OC, and BC) across the Himalaya (covering Indian, Nepal, and Bhutan parts); (ii) investigate the spatio-temporal dynamics of the emissions; and (iii) link the estimated emissions with meteorological conditions, to depict the regions of influence.

2. Study Area

The emissions from forest and grassland fires were quantified over the entire Himalaya of India (including the western and eastern Himalaya), Nepal, and Bhutan. The study area is characterized by diverse topography, i.e., from the riverine flood plain to high mountain peaks, ridges, and narrow valleys (Figure 1a). The climate of the study area widely varies from the western to eastern and southern to the northern part of the Himalaya due to the wide extent and physiographic variations. There is a hot humid, subtropical type (highest temperature and precipitation recorded between June and August), with a mild winter climate, found over the eastern Himalaya. The main active forest fire episodes occurred between March and April in this region. On the other hand, in the western and Nepal Himalaya, the climatic condition varies between tropical and temperate mountains, and the highest temperature is found from May to July. The peak fire activities in this region are concentrated between April and June [37]. The dominating forest types of the study area are evergreen broadleaf (EBF), evergreen needleleaf (ENF), deciduous broadleaf (DBF), and mixed forest (MF) (Figure 1b).

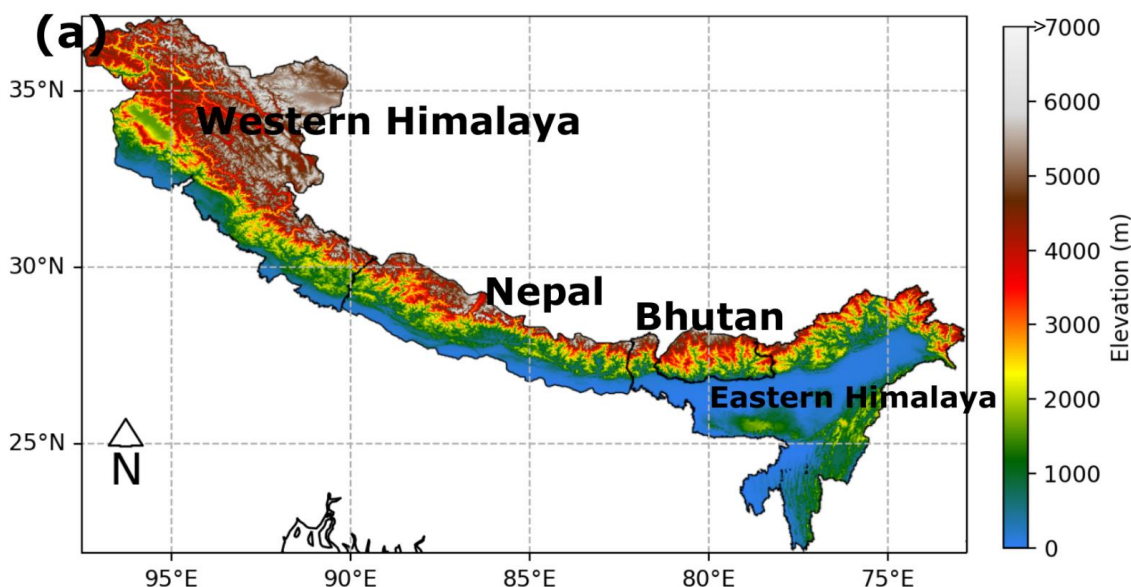


Figure 1. Cont.

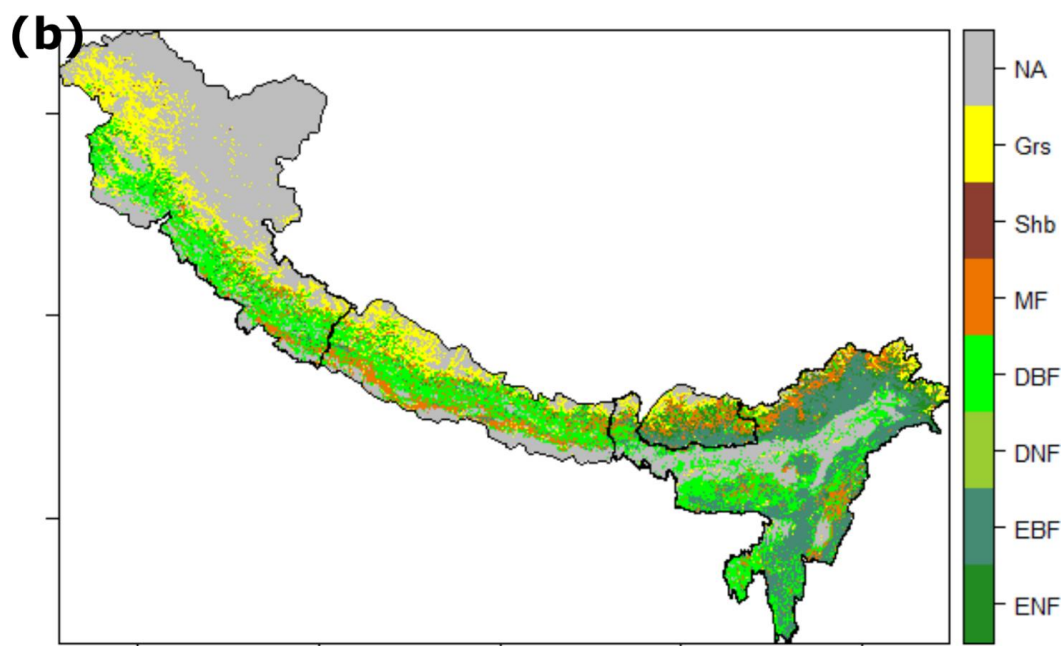


Figure 1. Elevation over study area including Western Himalaya, Nepal, Bhutan, and Eastern Himalaya (a) (Data source: Advanced Land Observation Satellite World 3D (30 m) digital surface model (DSM) and MODIS-derived forest cover map for 2010 (b); ENF: evergreen needleleaf forest, EBF: evergreen broadleaf forest, DNF: deciduous needleleaf forest, DBF: deciduous broadleaf forest, MF: mixed forest, Shb: shrubland, and Grs: grassland.

3. Materials and Methods

The forest fire emissions (CO , CO_2 , CH_4 , NO_x , SO_2 , NH_3 , $\text{PM}_{2.5}$, PM_{10} , OC, and BC) were estimated using satellite-derived datasets, i.e., burn area (km^2), biomass load (kg/m^2), combustion efficiency and emissions factors [27,53]. The function of emissions calculation is given below.

$$\text{Emissions} = \sum_{i=1}^n BA \times F \times CE \times EF \quad (1)$$

where i and BA denote the forest type and burn area; F and CE are dry biomass load and combustion efficiency (ratio between actual combusted and available fuel loads (unitless)), respectively; EF is emission factors, i.e., emission of a component per unit of dry matter combustion (g kg^{-1}). The methodological roadmap of the study is presented in Figure 2. The datasets used to accomplish the emissions estimation are listed in Table 1.

Table 1. List of the datasets used to accomplish the pixel-based estimation of forest fire emissions.

Data	Product ID	Characteristics	Source
Burn area	MCD64A1 v006	Monthly and 500 m	Land Processes Distributed Active Archive Center (LP DAAC)
Land Use Land Cover		Decadal and 100 m	EarthData https://earthdata.nasa.gov/ (accessed on 22 June 2022)
Biomass		1 km	GEOCARBON global biomass http://lucid.wur.nl/ (accessed on 22 June 2022)
Normalized Difference Vegetation Index (NDVI)	MOD13A2	16 Days and 1 km	NASA LP DAAC https://lpdaac.usgs.gov/ (accessed on 22 June 2022)
Percent Tree Cover	MOD44B	Yearly and 250 m	
Emission Factors			[3,7,26,35,54–56]
Global Fire Emissions Database, Version 4.1s	GFEDv4.1s	Monthly and 0.25°	ORNL DAAC https://daac.ornl.gov/ (accessed on 22 June 2022)
Meteorological (Wind Vector)		Hourly and 0.1°	ECMWF https://www.ecmwf.int/ (accessed on 22 June 2022)

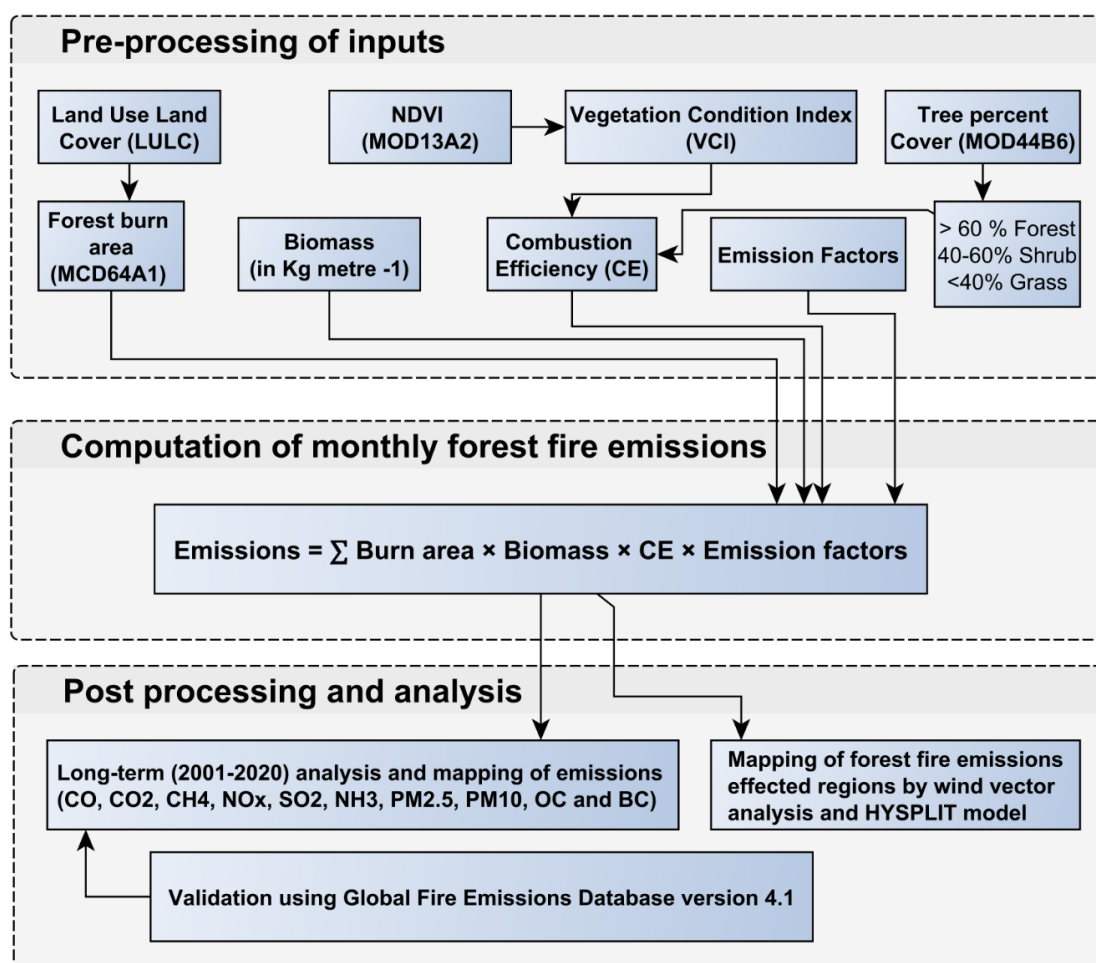


Figure 2. The methodology roadmap of forest fire emissions estimation and validation.

3.1. Land Use Land Cover (LULC)

The forest type information was retrieved from the global available Moderate Resolution Imaging Spectroradiometer (MODIS) yearly Land Use Land Cover (LULC) product (i.e., MCD12Q1; version 006). The MCD12Q1-based LULC has several classification schemes. The present study used International Geosphere-Biosphere Programme (IGBP), which comprises 17 classes [57]. According to this LULC scheme, evergreen broadleaf, evergreen needleleaf, deciduous broadleaf, deciduous needleleaf, and mixed forest are the forest composition of the study area. The study also considers the shrub (closed or open shrubland) and grass (including savannas) land cover. The aforementioned forest types (including shrub and grassland) were used to categorize the burn areas and to calculate the forest-specific emissions.

3.2. Burn Area

The burn area (BA) product MCD64A1 version 006 was obtained from MODIS which is available in 500 m spatial and monthly temporal resolution. MCD64A1 uses a hybrid algorithm that applies a dynamic threshold to composite imagery generated from a burn-sensitive vegetation index (VI), MODIS active fire observation (1 km), and landcover information. VIs are produced from atmospherically corrected surface reflectance products of bands 5 and 7, which are near-infrared (NIR) and shortwave infrared (SWIR), respectively [49]. In comparison with MODIS BA collections 5 and 5.1 (earlier versions), this fire product reduces false alarms and uncertainties [58]. Different fire-type observation data were used to validate the MCD64A1 burn area dataset worldwide [59].

3.3. Biomass

The above-ground biomass was obtained from the GEOCARBON global biomass dataset [28]. This dataset was produced by merging and harmonizing biomass maps of [60,61] over the pan-tropical region with a spatial resolution of 1 km using independent field observations and locally calibrated high-resolution maps [25]. This pan-tropical biomass map was integrated with the boreal forest biomass into GEOCARBON global forest biomass [62]. The BIOMASAR algorithm has used the hyper temporal observation of Envisat Advanced Synthetic Aperture Radar (ASAR) backscattered to estimate the spatial forest growing stock volume (GSV) over the boreal forest of the northern hemisphere. The ASAR-based estimations are spatially well captured GSV over the four ecological regions, i.e., polar, boreal, temperate, and sub-tropical [63]. The original downloaded biomass map was in Mg/ha unit and World Geodetic System (WGS84) projection system. For the study's purpose, the biomass value is converted to kg/m² unit. The scale of biomass varies from 0 to 60 kg/m² from the western to the eastern Himalaya (Figure S1), and the higher biomass is mainly exhibited over northern parts of the eastern Himalaya (including Bhutan) from dense evergreen broadleaf and needleleaf forest types.

3.4. NDVI and Tree Cover Percent

The MODIS TERRA-derived 16 days NDVI (MOD13A2 v006) level 3 and yearly percent tree cover (MOD44B v006) datasets were downloaded from the Google Earth Engine (GEE) repository after masking the quality assurance (QA) pixels. The MOD13A2 was derived from a daily composite of atmospherically corrected and bidirectional surface reflectance data [64]. A sub-pixel level representation of the vegetation cover of the ground surface is expressed as a percentage (0 to 100%) in MOD44B, where 100 represents a dense forest and 0 represents no vegetation cover. The yearly percentage tree cover is produced using the monthly composite of surface reflectance (including land surface temperature) of Terra MODIS 250 m and 500 m data [65].

3.5. Wind Vector Data

The wind vector data from the European Centre for Medium-range Weather Forecasting (ECMWF) ERA5-Land at hourly scale and 1000 hPa and 950 hPa pressure levels were used to assess the wind speed and direction during high forest fire months (Table 1).

3.6. Combustion Efficiency (CE)

The combustion efficiency (CE) is a ratio between the actually combusted and the available amount of fuel load. It mainly depends on the fuel type and moisture content [66]. The CE significantly varies across different fuel types and biomes. Usually, CE is considered a constant value, which is a source of bias in emission estimation and produces significant uncertainties. Previous studies used the fraction of tree cover (T_c) to define the spatio-temporal variabilities of CE, which assumes the CE is consistent with the landcover types (e.g., forest, grassland, and crop) [67–69]. The pixel-wise CE was calculated as a function of T_c as suggested by [7] and modified by [9]. We retrieved T_c from MODIS vegetation continuous fields (VCF) data, i.e., percentage tree cover (MOD44B v006). Based on the T_c , the fuel types have been divided into three categories, namely, forest (>60%), shrubland (40–60%), and grassland (<40%) [70]. These classes are reliable with the classification of [71].

The fuel moisture condition was considered in the forest CE (CE_f) calculation. To incorporate the fuel moisture condition, we used the monthly MODIS-based VCI, which is reliable for calculating CE in various continental forests [72]. The monthly VCI was calculated from MODIS-based NDVI (MOD13A2 v006) [35] over two decades (2001–2020) on 1 km spatial scale:

$$VCI = 100 \times \frac{NDVI_i - NDVI_{min}}{NDVI_{max} - NDVI_{min}} \quad (2)$$

where $NDVI_i$ is the $NDVI$ of the given month, and $NDVI_{min}$ and $NDVI_{max}$ are the corresponding minimum and maximum $NDVI$ of every year, respectively. The VCI ranges from 0 to 100, divided into six equal fuel moisture categories, i.e., very dry, dry, moderate, moist, wet, and very wet [35]. After that, the monthly variations of moisture conditions were traced by incorporating the fuel moisture category factors (mcf) in the CE calculation. The value of mcf increases from dry to wet fuels condition (i.e., very dry = 0.33, dry = 0.5, moderate = 1, moist = 2, wet = 4, and very wet = 5) [9,73]. The mcf is only used in forest CE estimation, while in shrubland and grassland CE , the T_c and VCI were used, respectively [70].

$$CE_f = (1 - e^{-1})^{mcf} \quad T_c > 60\% \quad (3)$$

The shrubland CE (CE_s) of the herbaceous region was calculated as a function of T_c according to Ito and Penner (2004) [9,70].

$$CE_s = \exp(-0.013 \times T_c) \quad 40\% < T_c \leq 60\% \quad (4)$$

According to [70], the grassland CE (CE_g) is determined by the percentage of green grass compared to total grass, which could be quantified by satellite-measured grassland VCI .

$$CE_g = \frac{1}{100} \times (-2.13 \times VCI + 138) \quad (5)$$

Finally, we combined all the computed land cover-wise (forest, shrubland, and grassland) CE s to derive the pixel-wise CE from every month over the whole study area. An average monthly (2001–2020) CE was measured and presented in Figure S2.

3.7. Emissions Factors (EFs)

The emission factors (EFs) refer to the amount of particular pollutants emitted from biomass burning [3,25,35,74]. EFs are a set of constants with a certain range of uncertainties. Here, we obtained EFs for different pollutants (gases and aerosols) in various biomass categories (forest types) from published studies over tropical and extra-tropical regions (Table 2) [3,7,35,54–56,74].

Table 2. Emissions factors (EFs; $g \text{ kg}^{-1}$) and uncertainties of pollutants (gases and aerosols) by different forest types.

Forest Types	CO	CO ₂	CH ₄	NO _x	SO ₂	NH ₃	PM _{2.5}	PM ₁₀	OC	BC
EBF	92.0 (±27)	1663.0 (±58)	5.1 (±2.0)	2.6 (±1.4)	0.5 (±0.2)	0.8 (±1.2)	9.7 (±3.5)	13.86	4.7 (±2.7)	0.5 (±0.3)
ENF	118 (±45)	1514.0 (±121)	6 (±3.1)	1.8 (±0.7)	1.0 (±0.3)	3.5 (±2.3)	13.0 (±5.9)	18.57	7.8 (±4.8)	0.2 (±0.2)
DBF	102 (±19)	1630.0 (±37)	5.0 (±0.9)	1.3 (±0.6)	1.0 (±0.3)	1.5 (±0.4)	13.0 (±5.6)	18.57	9.2 (±4.8)	0.6 (±0.2)
DNF	118 (±45)	1514.0 (±121)	6.0 (±3.1)	3.0 (±0.7)	1.0 (±0.3)	3.5 (±2.3)	13.6 (±5.9)	19.43	7.8 (±4.8)	0.2 (±0.2)
MF	102.0 (±19)	1630.0 (±37)	5.0 (±0.9)	1.3 (±0.6)	1.0 (±0.3)	1.5 (±0.4)	13.0 (±5.6)	18.57	9.2 (±4.8)	0.6 (±0.2)
Shrub	68.0 (±17)	1716.0 (±38)	2.6 (±0.9)	3.9 (±0.8)	0.7 (±0.3)	1.2 (±0.4)	9.3 (±3.4)	13.29	6.6 (±1.2)	0.5 (±0.2)
Grass	59.0 (±17)	1692.0 (±38)	1.5 (±0.9)	2.8 (±0.8)	0.5 (±0.3)	0.5 (±0.4)	5.4 (±3.4)	7.71	2.6 (±1.2)	0.4 (±0.2)

3.8. Global Fire Emission Dataset

The Global Fire Emission Dataset version 4.1s (GFEDv4.1s) is a joint dataset of vegetation fire activities and productivity which estimates the monthly global scale burn area and fire emissions in 0.25° grid cell [56,75]. This version of GFEDv4.1s has incorporated the small fire patches from the MODIS burn area product, improving emission estimation accuracy. The present study has used this dataset to compare and validate the estimated emissions over the Himalaya.

3.9. HYSPLIT Model

A wind forward trajectory model, i.e., Hybrid Single-Particle Lagrangian Integrated Trajectory (HYSPLIT), was also performed to track the path of the air parcels blown from the high fire location [76]. The HYSPLIT was computed at NOAA's Air Resource Laboratory (ARL; Website: <https://www.ready.noaa.gov/HYSPLIT.php>; accessed on 22 June 2022) in 2016 and 2018 at various high fire times and locations.

4. Results

4.1. Variability of Forest Burn Area

The forest fire burn area significantly varies with space and time over the entire study area. The average (2001–2020) forest burn area fraction was substantially varied from the western Himalaya to the central Himalaya (Nepal) and the eastern Himalaya (including Bhutan and India part). The higher burn area fraction (0.7 to 1 km²) patches were found over southeastern parts of the eastern Himalaya, southern parts of the central Himalaya, and southeastern parts of the western Himalaya (Figure 3a,b). The average annual burn area over the last two decades (2001–2020) was 5557.35 km² with a considerable size of variability (standard deviation (σ) = 2661.71 km²). In the first decade (2001–2010), the annual burn area showed a significant increasing trend of 755.7 km² year⁻¹ ($p = 0.01$), while in the next decade (2011–2020) it showed a decreasing trend of -286.5 km² year⁻¹ ($p = 0.30$) (Figure 3c).

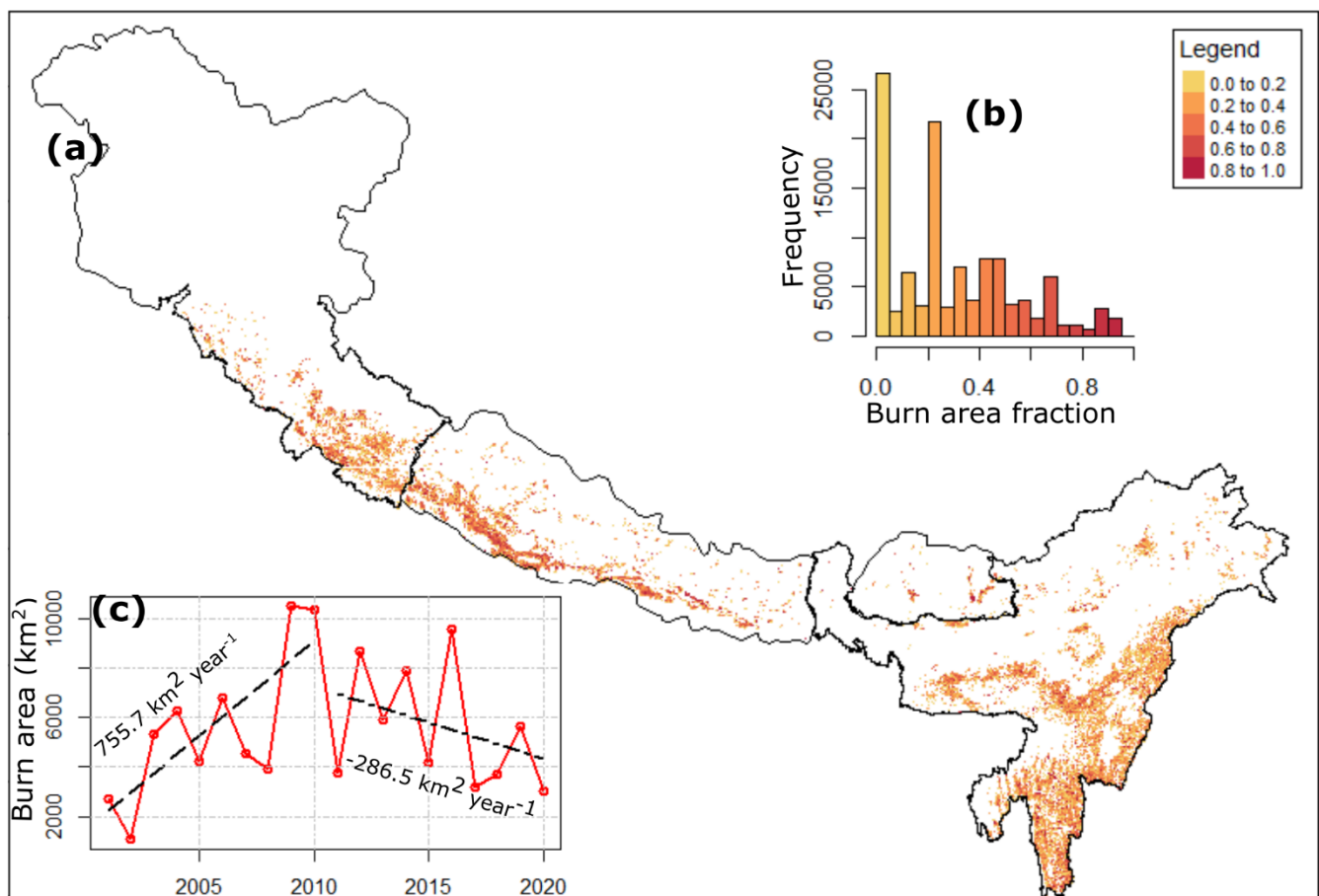


Figure 3. Annual average (2001–2020) forest fire burn area fraction (km²) in a 1 × 1 km grid over the study area (a), the corresponding histogram of burn area fraction (b), and inter-annual variability of forest burn area (km²) (c).

4.2. Inter-Annual Variations of Forest Fire Emissions

The emissions such as CO, CO₂, CH₄, NO_x, SO₂, NH₃, PM_{2.5}, PM₁₀, OC, and BC from forest fire were computed over the Himalaya. Out of these pollutants, the highest emitted pollutant was CO₂ from forest fires (including shrubs and grass). The average (\bar{x}) and variability (standard deviation; σ) of CO₂ emissions from forest fire has reasonably varied from the western to the eastern part of the Himalaya. The highest annual average CO₂ emission was found in the eastern Himalaya ($\bar{x} = 20.37$ and $\sigma = 14.56$ Tg) followed by Nepal ($\bar{x} = 15.52$ and $\sigma = 12.39$ Tg) and the western Himalaya ($\bar{x} = 4.92$ and $\sigma = 3.9$ Gg) (Figure 4). The inter-annual variations of all the pollutants are listed in Tables S1–S3. The annual average emissions of all 10 pollutants are presented in Table 3. Over the entire study area, the annual average emissions from 2001 to 2020 were 2.52 Tg of CO ($\sigma = 1.33$); 40.81 Tg of CO₂ ($\sigma = 21.52$); 0.13 Tg of CH₄ ($\sigma = 0.07$); 0.04 Tg of NO_x ($\sigma = 0.02$); 0.023 Tg of SO₂ ($\sigma = 0.012$); 0.036 Tg of NH₃ ($\sigma = 0.019$); 0.312 Tg of PM_{2.5} ($\sigma = 0.164$); 0.45 Tg of PM₁₀ ($\sigma = 0.24$); 0.21 Tg of OC ($\sigma = 0.11$); and 0.014 Tg of BC ($\sigma = 0.008$). The inter-annual variations of the emissions over the entire study area have significant variability (Figure S3).

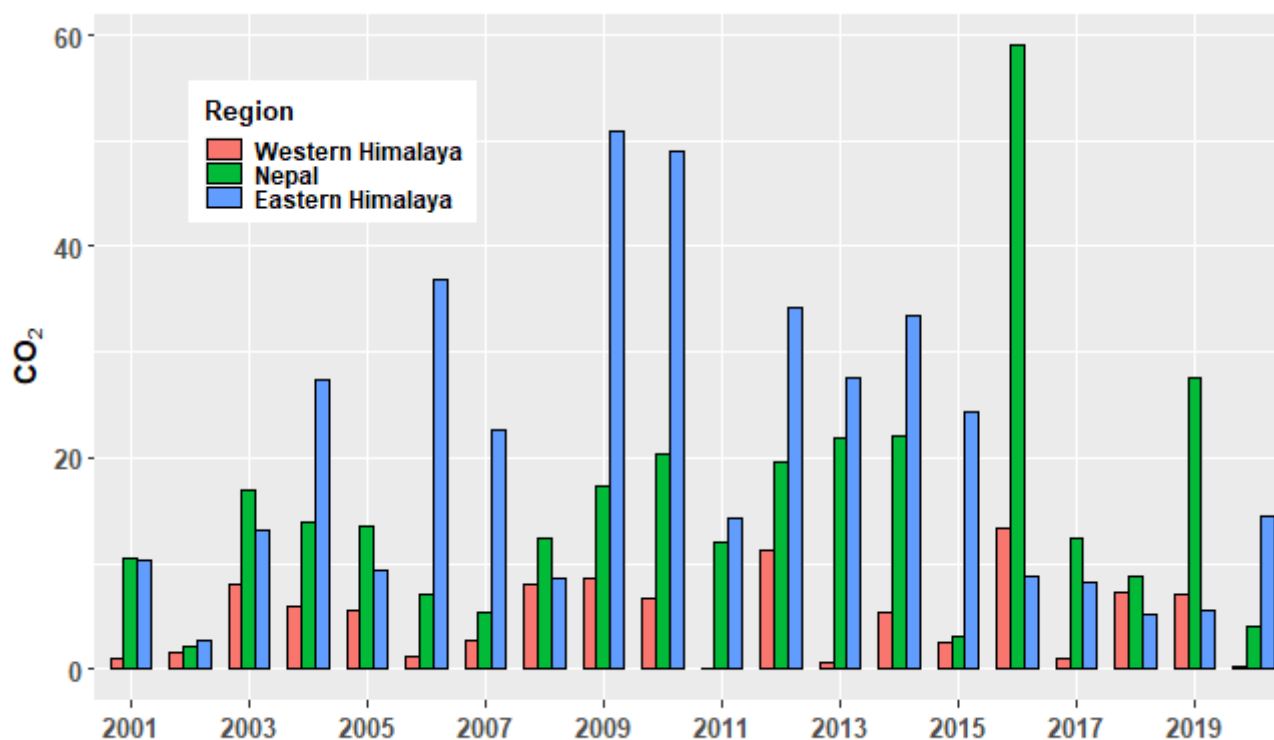


Figure 4. Inter-annual (2001–2020) variations of emissions (Tg) from forest fire over western to eastern Himalaya.

Table 3. The annual average and stand deviation of emissions (Tg year⁻¹) from forest fire over the Himalaya.

Regions	CO	CO ₂	CH ₄	NO _x	SO ₂	NH ₃	PM _{2.5}	PM ₁₀	OC	BC
Western Himalaya	0.32 (±0.25)	4.92 (±3.90)	0.016 (±0.012)	0.004 (±0.0033)	0.003 (±0.002)	0.005 (±0.004)	0.04 (±0.03)	0.06 (±0.04)	0.027 (±0.021)	0.0017 (±0.0013)
Nepal	0.97 (±0.78)	15.52 (±12.39)	0.048 (±0.038)	0.013 (±0.010)	0.009 (±0.008)	0.014 (±0.011)	0.124 (±0.098)	0.176 (±0.141)	0.087 (±0.069)	0.006 (±0.005)
Eastern Himalaya	1.23 (±0.88)	20.37 (±14.56)	0.063 (±0.045)	0.021 (±0.015)	0.011 (±0.007)	0.016 (±0.011)	0.149 (±0.106)	0.213 (±0.151)	0.098 (±0.068)	0.007 (±0.005)

With respect to all the selected emissions species, the eastern Himalaya exhibited the highest amounts of emissions, as the forest burn area was higher in this region. In

the case of the western Himalaya, the deciduous broadleaf and mixed forest type fires emitted the highest fire emissions (45.62% and 41.23%), followed by evergreen needle and broadleaf forest (11.23% and 1.91%), in respect of all 10 selected pollutants. In Nepal, the fire emissions from deciduous broadleaf forest (19.44%) were lower than mixed forest (79.16%). On the other hand, evergreen broadleaf forest fires in the eastern Himalaya emitted 29.98% of pollutants, lower than deciduous broadleaf forest (57.23%) and higher than mixed forest (12.43%) (Figure 5).

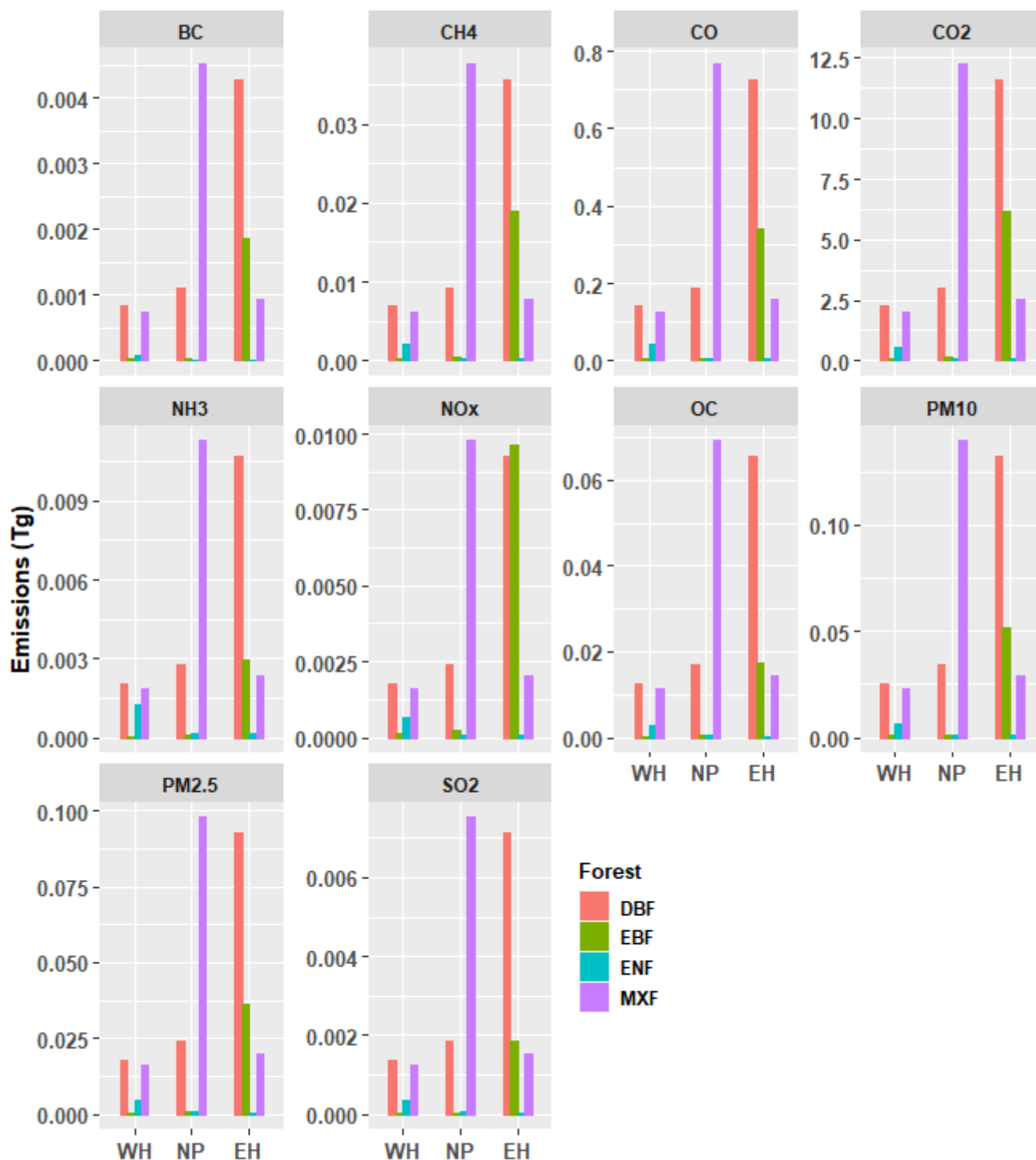


Figure 5. Forest type-wise annual (2001–2020) average emissions (Tg year⁻¹) over the study area (WH: Western Himalaya, NP: Nepal, and EH: Eastern Himalaya).

4.3. Spatial Distributions of Emissions

The emissions from the different forest categories were estimated over a 1 km grid. We observed distinct and similar spatial patterns of emissions, albeit in different degrees, over the study area. To unfold the spatial distribution pattern of forest fire emissions, we have used the example of CO₂ and CO (Figure 6a,b). The higher CO₂ (0.01–0.02 Tg year⁻¹) and CO (0.007–0.002 Tg year⁻¹ in each grid cell) emissions were detected along the south-eastern parts of the the eastern Himalaya, southern regions of Nepal, and south-eastern parts of the western Himalaya. The lower emissions pixels/patches were scattered towards some of the northern higher elevation regions of the western Himalaya, Nepal, and north-western parts of the eastern Himalaya.

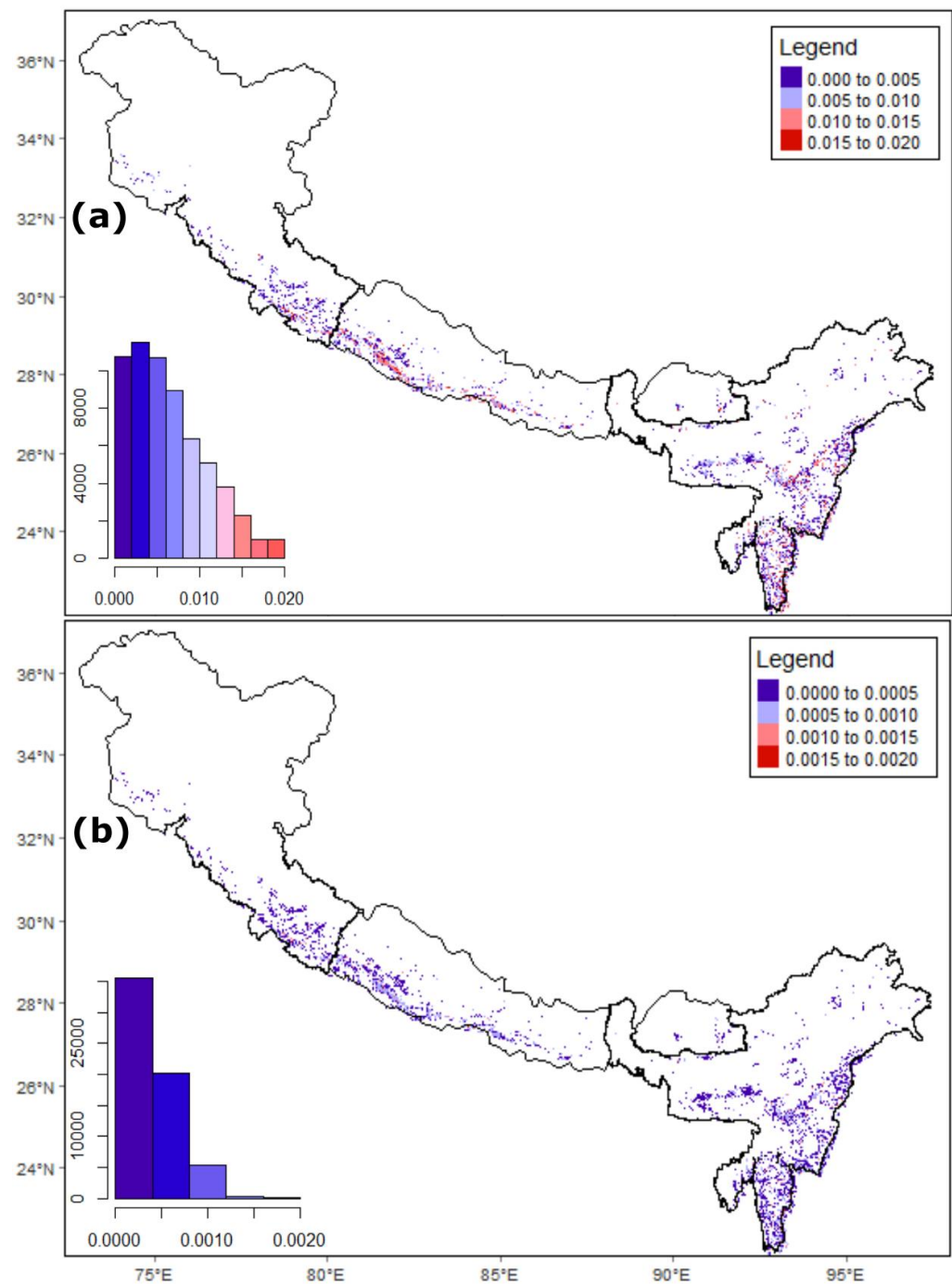


Figure 6. The spatial distribution of annual average (2001–2020) CO₂ (a) and CO (b) in Tg/km², including all the forest categories.

4.4. Temporal Trend of Emissions

The temporal patterns of forest fire emissions of all the species demonstrated similar and consistent annual variations from 2001–2020 over the study area. The highest emission was recorded in 2016, followed by 2009 and 2010 (Figure S3). From forest fires, 81.03, 77.00, and 67.05 Tg of total CO₂ were released in 2016, 2009, and 2010, respectively. The annual trend of the emissions was quantified using a linear function; the magnitude of the trend in Tg (β), significant level (p), and coefficients of determination (R^2) are presented in Table 4. In the first decade, i.e., 2001–2010, there was a significant positive trend in forest fire emissions. The CO₂ increased at the rate of 5.49 Tg year⁻¹ in the first decades. In contrast, a downward trend in emissions was recorded in the next decade (2011–2020), but only the OC emission trend reached up to a significant level ($p < 0.05$) (Table 4).

Table 4. Decadal linear trends (Tg year⁻¹) of forest fire emissions over the entire study area.

Emissions in Tg	2001–2010			2011–2020		
	β (Trend)	p	R^2	β (Trend)	p	R^2
CO	0.333	0.015 *	0.54	−0.165	0.293	0.14
CO ₂	5.468	0.015 *	0.54	−2.738	0.276	0.15
CH ₄	0.017	0.015 *	0.54	−0.008	0.279	0.14
NO _x	0.005	0.015 *	0.55	−0.003	0.191	0.2
SO ₂	0.003	0.016 *	0.54	−0.001	0.346	0.11
NH ₃	0.004	0.017 *	0.53	−0.002	0.356	0.11
PM _{2.5}	0.041	0.016 *	0.54	−0.02	0.311	0.13
PM ₁₀	0.058	0.016 *	0.54	−0.029	0.311	0.13
OC	0.057	0.035 *	0.45	−0.012	0.794	0.01 *
BC	0.002	0.015 *	0.54	−0.001	0.293	0.14

The asterisk mark (*) shows significant trends over 95%.

4.5. Comparison with Other Measures and Uncertainties

The pixel-based estimated forest fire emissions of CO₂, CO, OC, BC, CH₄, and NO_x were compared with the Global Fire Emission Dataset version 4.1s (GFEDv4.1s). The annual average and standard error (2001–2020) of the aforementioned emissions of this study and GFEDv4.1s were plotted in Figure 7. Except for NO_x, all the emissions from this study (i.e., CO₂, CO, OC, BC, and CH₄) were comparatively higher than in the GFEDv4.1s. The highest difference was found in OC emissions over the study area. This difference might be attributed to the different inputs (especially biomass and CE) in emissions estimation. The statistical association between the estimated emissions of this study and GFEDv4.1s (Table 5) showed a significantly promising association where the Pearson correlation coefficient (r) ranges from 0.8 to 0.93. In the case of CO₂, the root mean square error (RMSE) and mean absolute error (MAE) between the estimated and GFEDv4.1s were demonstrated at 5.93 Tg and 9.33 Tg, respectively.

Table 5. The statistical association between the estimated emissions from forest fire and the GFED4.1s-derived emissions (in Tg).

Species	r	R^2	p	RMSE (Tg)	MAE (Tg)
CO ₂	0.93	0.86	<0.01 *	5.93	9.33
CO	0.92	0.85	<0.01 *	0.73	0.77
OC	0.80	0.64	<0.01 *	0.16	0.34
BC	0.93	0.86	<0.01 *	0.003	0.005
CH ₄	0.91	0.84	<0.01 *	0.025	0.052
NO _x	0.92	0.85	<0.01 *	0.007	0.014

* denotes confidence level over 99%.

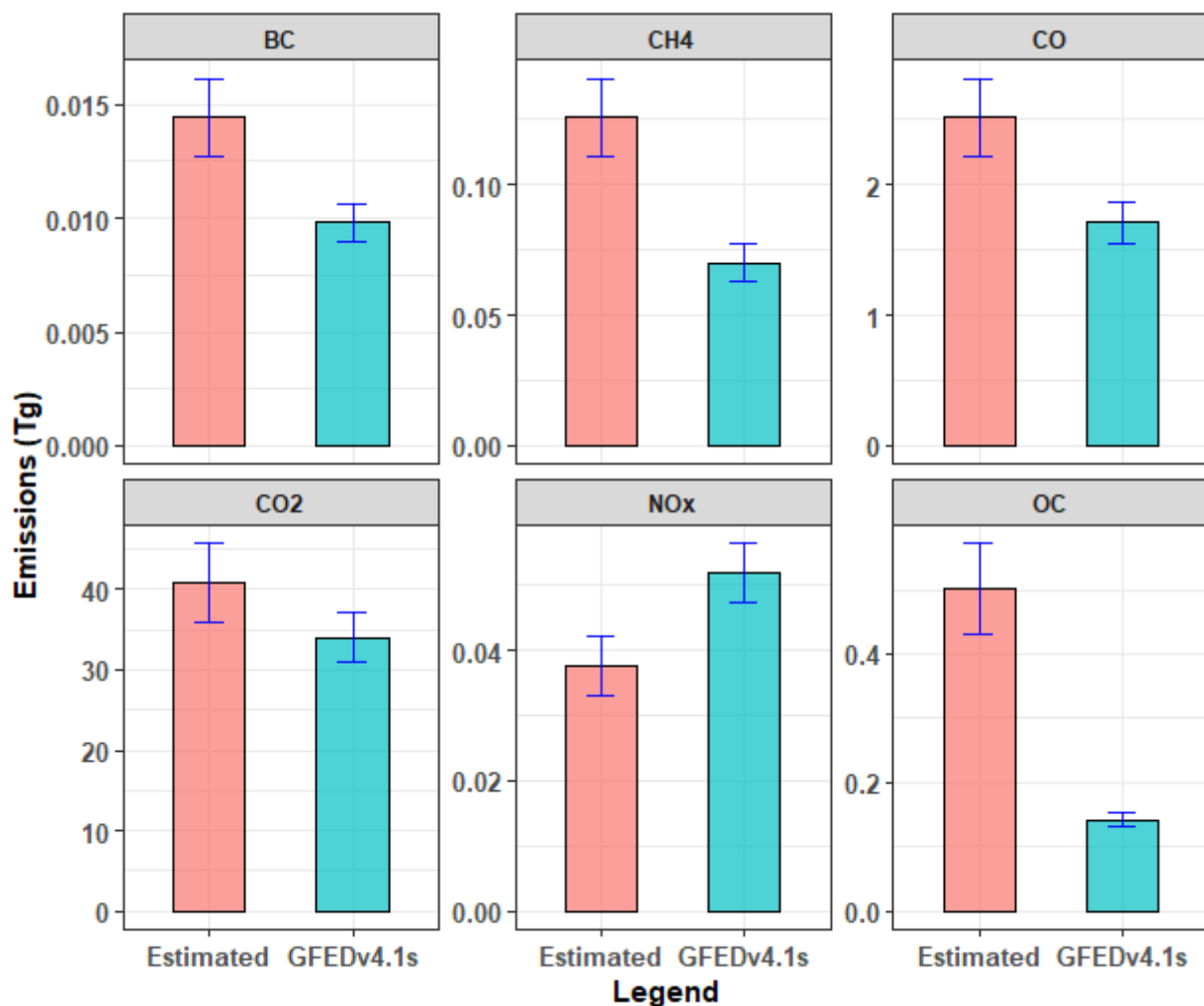


Figure 7. Comparison of annual averaged (2001–2020) emissions from Global Fire Emissions data version 4.1s (GFED v4.1s) with the pixel-based computed emissions of this study (Estimated). The error bar is based on the standard error of annual emissions.

5. Discussion

The Himalayan belt is a fragile ecosystem with mountainous topography that witnessed a significant number of forest fire incidents over the last two decades (2001–2020). The present study found a substantial interannual variability of forest fire activities over the Himalaya. There is also strong seasonal control of forest fire activities, as the pre-monsoon season (February to June) is the main forest fire period. However, the peak fire time varies from the western to eastern Himalaya. The highest forest fire emissions were seen in March, April, and May over the study area (Figure S4). The key findings of this study indicate that the forest fire emissions and forest burn area significantly increased during the decade 2001–2010, but in the next decade (2011–2020) there was a decreasing trend. The average annual (2001–2020) CO₂ and CO emissions from forest fires were 40.81 Tg and 2.52 Tg over the entire study area, with the maximum forest fire emissions in 2016, 2009, and 2010. The above results are consistent with an independent dataset (GFED 4.1) that revealed the highest emissions over these years (especially in 2009 and 2010) (Figure S5). Few previous studies over parts of the Himalaya have recorded high fire activities and forest fire emissions in these aforementioned years [37,41,77,78]. The eastern Himalaya recorded the highest emissions with an average annual CO₂ emission of 20.37 Tg, followed by Nepal (15.52 Tg) and the western Himalaya (4.92 Tg), due to higher burn area in the EBF, DBF, and MF regions over the eastern and Nepal Himalaya. Studying the forest type-wise emissions

showed that MF, DBF, and EBF, respectively, have produced higher emissions. Spatially, the south-eastern part of the western and eastern Himalaya and the southern slope of Nepal revealed the highest forest fire emissions, which could be supported by the high fire activities of these regions. These regions have high proximity to the densely populated areas (mainly the Indo-Gangetic plain) of the western to eastern Himalaya (Figure S6). The previous studies based on ground-based and remote sensing-based measures also found a significant association between forest fire episodes and declining air quality over the western Himalayan region [40–42], the central Himalaya (Nepal) [79,80], and the eastern Himalaya [81].

The monthly average wind vector analysis (at a pressure level of 1000 hPa) of the high forest fire years 2010, 2016, and 2018 showed that the wind directions in the western Himalaya, Nepal, and eastern Himalaya are towards the south and south-east with a comparatively slow wind speed (Figure 8). This reflects the transportation of forest fire emissions towards the southern slope of the western and central Himalaya (i.e., Indo-Gangetic plain), a densely populated region of India. With respect to the wind vector plot at 950 hPa pressure level, most wind direction is south-eastern with a higher wind speed (Figure S7). This means that the high-energy forest fire smoke plumes would flow to the south-east and contribute to high altitudinal air pollution and long-range transport. Furthermore, we have traced the forward trajectory of air parcels using the Hybrid Single-Particle Lagrangian Integrated Trajectory model (HYSPPLIT) at the vertical levels of 100 m, 500 m, and 1000 m over high forest fire times in 2016 and 2018 (Figure 9). The western Himalayan forward trajectory of 2016 (29 April to 1 May) showed initial transportation towards the north-east, then south and south-east, while the trajectory of 2018 exhibited south-eastward transportation of air parcels (Figure 9a,b). The northward transported forest fire smoke might precipitate the pollutants over the high altitudinal glacial surface. The studies found significant correspondences between the depositions of BC (from biomass burning) over Himalayan glaciers (like Gangotri and Tapovan) and forest fire activities [43,45,82], which accelerates the melting rate of glaciers [46]. The forward trajectory over Nepal depicted eastward and north-eastward transportation, irrespective of the vertical level (Figure 9c,d). From the dense forest fire patches of the eastern Himalaya, mostly an eastward transportation of air parcels was recorded (Figure 9c,d).

Estimates of emissions from forest fires across a mountainous terrain are subject to relatively high uncertainties from burn area, biomass fuel, combustion efficiency, and forest-specific emission factors [25]. MCD64A1, a global fire product, has proven to be a reliable source for forest/wildfire burn area for open biomass burnings, although detection of small fires (<21 ha) is challenging from the 500 m pixels [59]. Moreover, the utilized biomass fuel layer has an uncertainty of up to 50% of the mean value [28]. In addition, the empirical method used to determine the monthly combustion factors has an uncertainty of 20–30% [35]. The study incorporated forest-specific emission factors for trace gases and aerosols from various literature, which might be a source of uncertainty in estimating forest fire emissions (Table 2) [25]. Due to the limited availability of such a large regional scale biomass dataset, the study utilized a single biomass dataset [28] to estimate emissions, and hence, some degree of uncertainty remained in emissions estimation. Therefore, further studies are required to get more accurate input datasets for more precise forest fire emissions estimation. However, the most significant aspect of this study is that it is the first of its kind, estimating forest fire emissions on a 1 km grid over the last two decades (2001–2020). Furthermore, this emissions inventory might be used in regional atmospheric pollution and biogeochemical circulation modelling to obtain more accurate atmospheric dynamics of emissions. It can also be valuable for policymakers when designing strategies for reducing emissions from fires to meet the challenges of climate change mitigation.

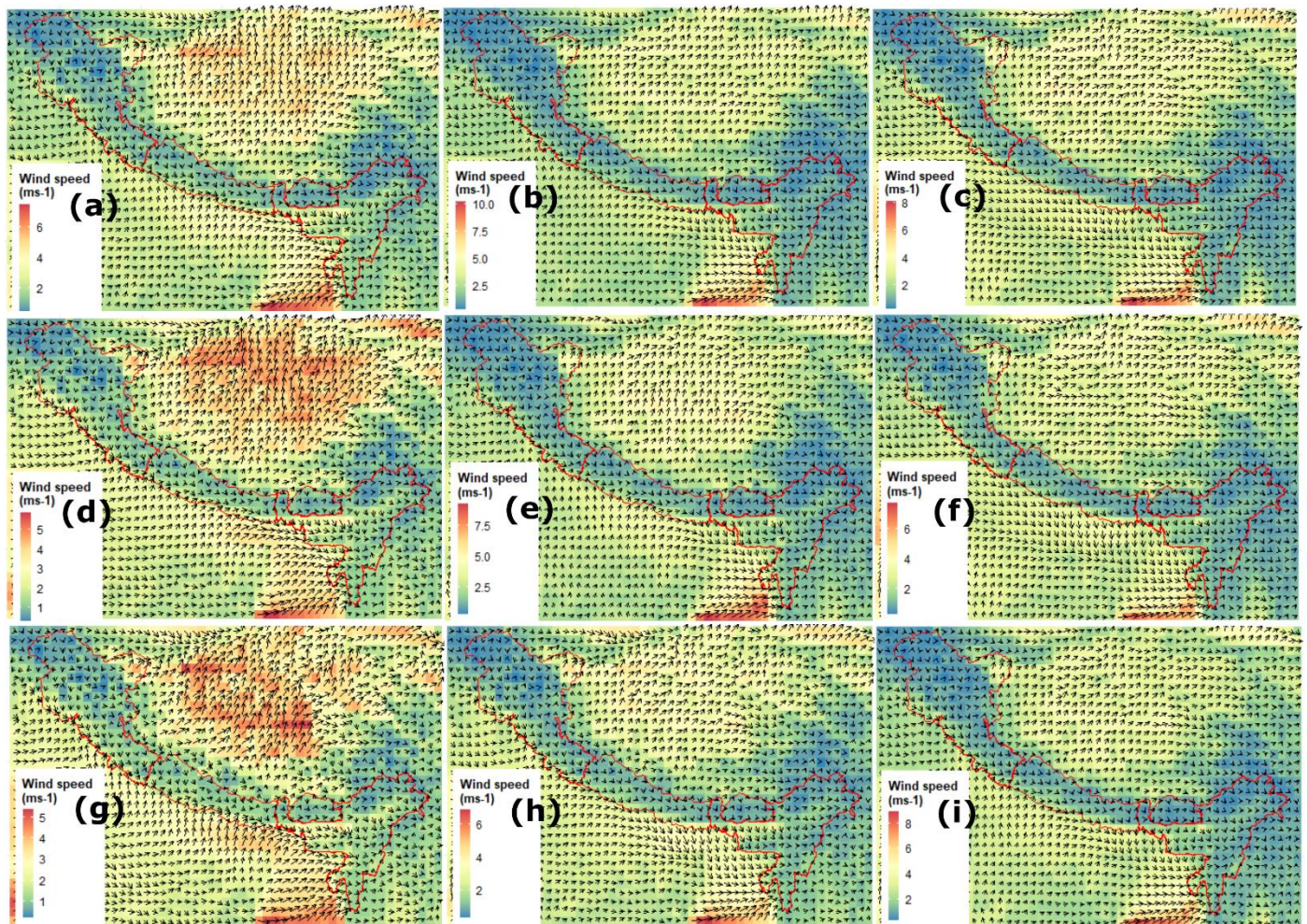


Figure 8. Wind vector plot on 1000 hPa pressure level for March, April, and May, respectively, in 1910 (a–c), 2016 (d–f), and 2018 (g–i).

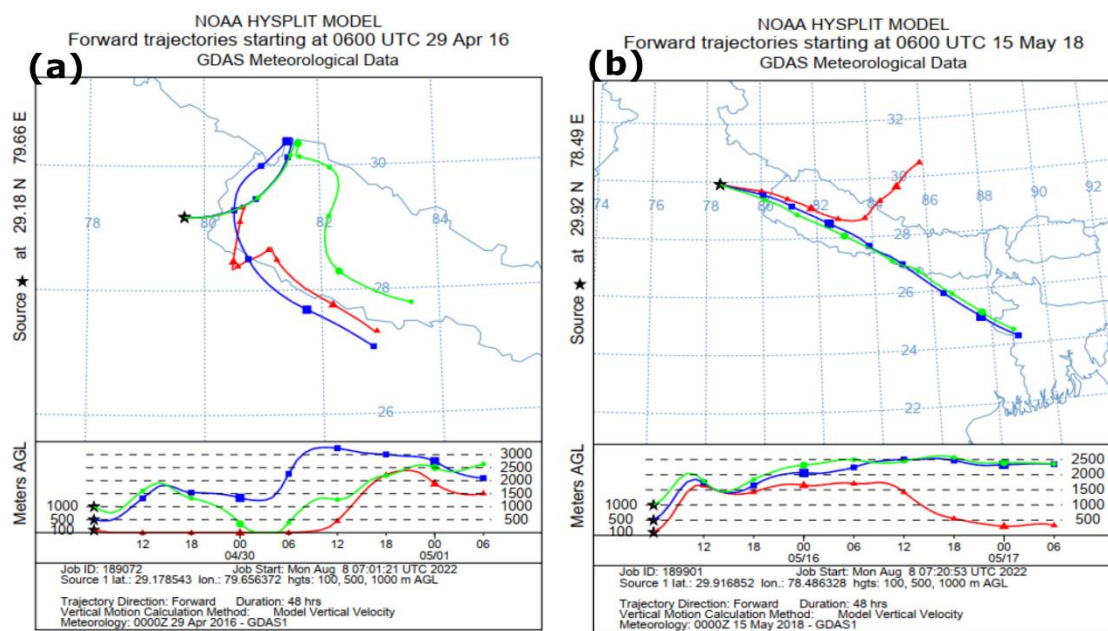


Figure 9. Cont.

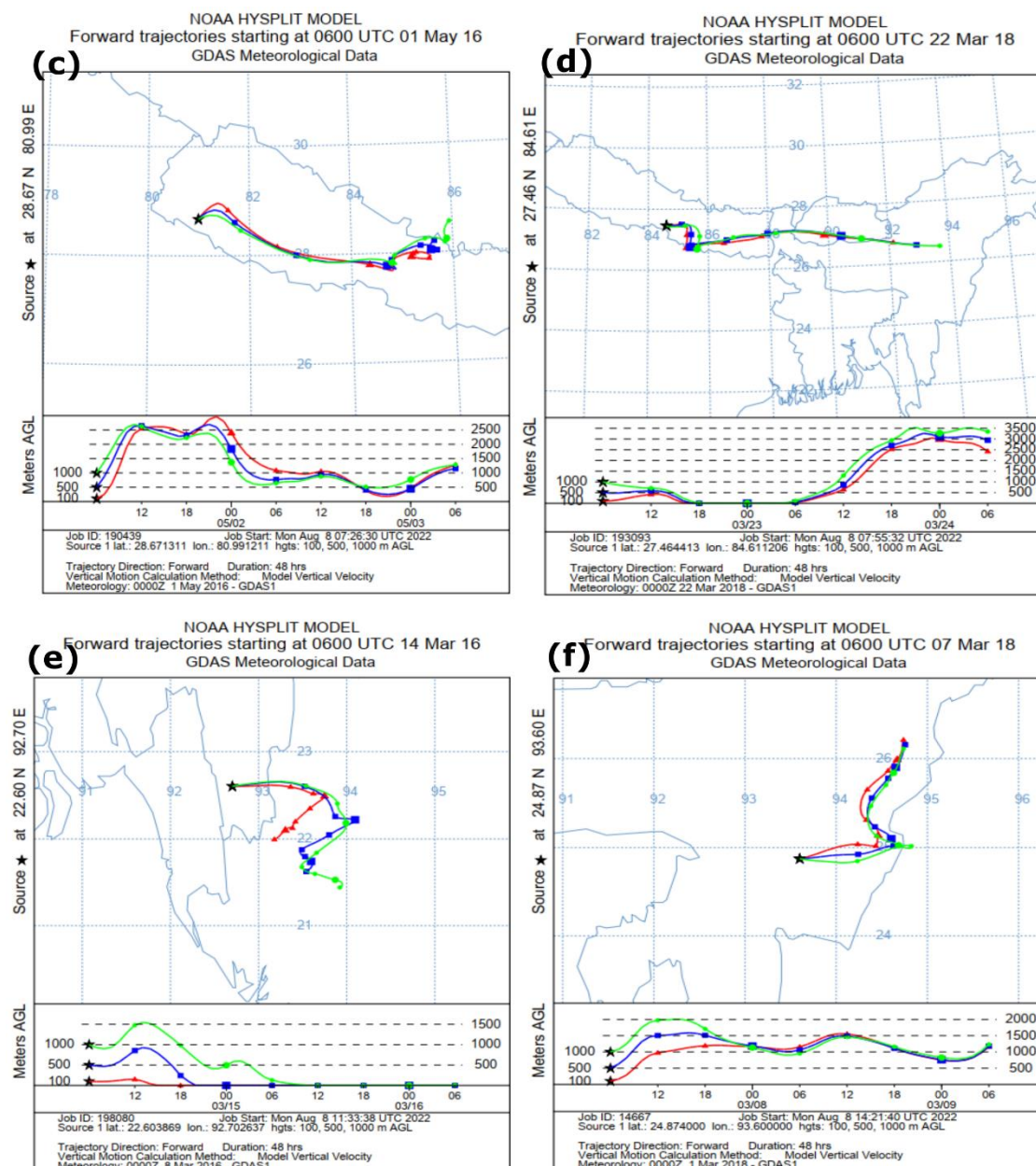


Figure 9. Forward Hybrid Single-Particle Lagrangian Integrated Trajectory model (HYSPLIT) on high forest fire locations of 2016 and 2018 over western Himalaya (a,b), Nepal (c,d), and eastern Himalaya (e,f).

6. Conclusions

The study found a significant spatial variation of emissions and the highest annual average CO₂ recorded in the eastern Himalaya (20.37 Tg year⁻¹), followed by Nepal (15.52 Tg year⁻¹) and the western Himalaya (4.92 Tg year⁻¹). The forest fire emissions over the Himalaya have had a significant interannual variability over the last two decades. However, the first decade exhibited increasing emissions but then there was a decreasing trend in the next decade (2011–2020). The mixed, deciduous broadleaf forest fire is responsible for the most emissions in the Himalaya, followed by the evergreen broadleaf forest fire. The southern slope of the western and central Himalaya (Nepal) and the south and south-eastern regions of the eastern Himalaya accounted for the highest forest fire fraction (0.7 to 1 km²) and emissions. Higher forest fire emissions were found in 2016, 2009, and 2010, and the peak emissions season corresponds to the pre-monsoon (i.e., March, April, and May). The locations of high emission regions are in higher proximity to the populated

areas of the western and eastern Himalaya, which contributes to deteriorating regional air quality and human health. Wind vector and trajectory analysis depict the direction and path of the forest fire emissions, i.e., mainly south and southeastward. This high-resolution emissions inventory and space-time dynamics in connection with wind vector analyses would provide a scientific and reliable basis for forest fire emission policy.

Supplementary Materials: The following supporting information can be downloaded at: <https://www.mdpi.com/article/10.3390/rs14215302/s1>, Figure S1: Above ground biomass (in kg/m²) map; Figure S2: Monthly average (2001–2020) of combustion efficiency (CE); Table S1: Inter-annual variations (2001–2020) of emissions in Tg over western Himalaya; Table S2: Inter-annual variations (2001–2020) of emissions in Tg over Nepal/Central Himalaya; Table S3: Inter-annual variations (2001–2020) of emissions in Tg over eastern Himalaya; Figure S3: Inter-annual variations of forest fire emissions from 2001–2020 over the entire study area; Figure S4: Average monthly (2001–2020) forest fire emissions over the study area; Figure S5: Annual forest fire emissions from Global Fire Emission Dataset 4.1 (GFED4.1) over Himalaya. Figure S6: Population density of 2015 (persons/km²) over the study area. Figure S7: Wind vector plot on 950 hPa pressure level of March, April and May.

Author Contributions: S.B.: Conceptualization, investigation, methodology, software, analysis, writing and editing original draft. B.R.P. and A.C.P.: Supervision, software, analysis, writing and editing original draft. N.K.: Supervision, review and editing. All authors have read and agreed to the published version of the manuscript.

Funding: This work was supported by the University Grants Commission under the NET-JRF fellowship number [3289/(SC NET-JAN 2017)]. Additionally, this work was supported by the Open Access Publication Fund of the University of Bonn, Germany.

Data Availability Statement: All the data used in the study are publicly available. The sources are properly mentioned in the data section, i.e., in Table 1. All data generated or analyzed during this study are included in this published article (and its Supplementary Materials).

Acknowledgments: The authors are thankful to the United States Geological Survey (USGS), Land Processes Distributed Active Archive Center (LP DAAC), for the freely available data.

Conflicts of Interest: The authors declare no conflict to interest.

References

1. Andreae, M.O.; Crutzen, P.J. Atmospheric Aerosols: Biogeochemical Sources and Role in Atmospheric Chemistry. *Science* **1997**, *276*, 1052–1058. [[CrossRef](#)]
2. van der Werf, G.R.; Randerson, J.T.; Giglio, L.; van Leeuwen, T.T.; Chen, Y.; Rogers, B.M.; Mu, M.; van Marle, M.J.E.; Morton, D.C.; Collatz, G.J.; et al. Global Fire Emissions Estimates during 1997–2016. *Earth Syst. Sci. Data* **2017**, *9*, 697–720. [[CrossRef](#)]
3. Andreae, M.O. Emission of Trace Gases and Aerosols from Biomass Burning—an Updated Assessment. *Atmos. Chem. Phys.* **2019**, *19*, 8523–8546. [[CrossRef](#)]
4. Bond, T.C.; Doherty, S.J.; Fahey, D.W.; Forster, P.M.; Berntsen, T.; DeAngelo, B.J.; Flanner, M.G.; Ghan, S.; Kärcher, B.; Koch, D.; et al. Bounding the Role of Black Carbon in the Climate System: A Scientific Assessment. *J. Geophys. Res. Atmos.* **2013**, *118*, 5380–5552. [[CrossRef](#)]
5. Levine, J.S. Global Biomass Burning: A Case Study of the Gaseous and Particulate Emissions Released to the Atmosphere During the 1997 Fires in Kalimantan and Sumatra, Indonesia. In *Advances in Global Change Research*; Springer: Dordrecht, The Netherlands, 2000; pp. 15–31. [[CrossRef](#)]
6. Ramanathan, V.; Carmichael, G. Global and Regional Climate Changes Due to Black Carbon. *Nat. Geosci.* **2008**, *1*, 221–227. [[CrossRef](#)]
7. Wiedinmyer, C.; Akagi, S.K.; Yokelson, R.J.; Emmons, L.K.; Al-Saadi, J.A.; Orlando, J.J.; Soja, A.J. The Fire INventory from NCAR (FINN): A High Resolution Global Model to Estimate the Emissions from Open Burning. *Geosci. Model Dev.* **2011**, *4*, 625–641. [[CrossRef](#)]
8. Hao, W.M.; Liu, M.-H. Spatial and Temporal Distribution of Tropical Biomass Burning. *Glob. Biogeochem. Cycles* **1994**, *8*, 495–503. [[CrossRef](#)]
9. Shi, Y.; Zhao, A.; Matsunaga, T.; Yamaguchi, Y.; Zang, S.; Li, Z.; Yu, T.; Gu, X. High-Resolution Inventory of Mercury Emissions from Biomass Burning in Tropical Continents during 2001–2017. *Sci. Total Environ.* **2019**, *653*, 638–648. [[CrossRef](#)]
10. Keywood, M.; Kanakidou, M.; Stohl, A.; Dentener, F.; Grassi, G.; Meyer, C.P.; Torseth, K.; Edwards, D.; Thompson, A.M.; Lohmann, U.; et al. Fire in the Air: Biomass Burning Impacts in a Changing Climate. *Crit. Rev. Environ. Sci. Technol.* **2013**, *43*, 40–83. [[CrossRef](#)]

11. Sannigrahi, S.; Pilla, F.; Maiti, A.; Bar, S.; Bhatt, S.; Kaparwan, A.; Zhang, Q.; Keesstra, S.; Cerda, A. Examining the Status of Forest Fire Emission in 2020 and Its Connection to COVID-19 Incidents in West Coast Regions of the United States. *Environ. Res.* **2022**, *210*, 112818. [[CrossRef](#)]
12. Langmann, B.; Duncan, B.; Textor, C.; Trentmann, J.; van der Werf, G.R. Vegetation Fire Emissions and Their Impact on Air Pollution and Climate. *Atmos. Environ.* **2009**, *43*, 107–116. [[CrossRef](#)]
13. Silva, R.A.; West, J.J.; Zhang, Y.; Anenberg, S.C.; Lamarque, J.-F.; Shindell, D.T.; Collins, W.J.; Dalsoren, S.; Faluvegi, G.; Folberth, G.; et al. Global Premature Mortality Due to Anthropogenic Outdoor Air Pollution and the Contribution of Past Climate Change. *Environ. Res. Lett.* **2013**, *8*, 034005. [[CrossRef](#)]
14. Taylor, D. Biomass Burning, Humans and Climate Change in Southeast Asia. *Biodivers. Conserv.* **2010**, *19*, 1025–1042. [[CrossRef](#)]
15. Cohen, A.J.; Brauer, M.; Burnett, R.; Anderson, H.R.; Frostad, J.; Estep, K.; Balakrishnan, K.; Brunekreef, B.; Dandona, L.; Dandona, R.; et al. Estimates and 25-Year Trends of the Global Burden of Disease Attributable to Ambient Air Pollution: An Analysis of Data from the Global Burden of Diseases Study 2015. *Lancet* **2017**, *389*, 1907–1918. [[CrossRef](#)]
16. Johnston, F.H.; Henderson, S.B.; Chen, Y.; Randerson, J.T.; Marlier, M.; DeFries, R.S.; Kinney, P.; Bowman, D.M.J.S.; Brauer, M. Estimated Global Mortality Attributable to Smoke from Landscape Fires. *Environ. Health Perspect.* **2012**, *120*, 695–701. [[CrossRef](#)]
17. WHO. Ambient (Outdoor) Air Pollution. Available online: [https://www.who.int/news-room/fact-sheets/detail/ambient-\(outdoor\)-air-quality-and-health](https://www.who.int/news-room/fact-sheets/detail/ambient-(outdoor)-air-quality-and-health) (accessed on 15 August 2022).
18. Trujano-Jiménez, F.; Ríos, B.; Jaramillo, A.; Ladino, L.A.; Raga, G.B. The Impact of Biomass Burning Emissions on Protected Natural Areas in Central and Southern Mexico. *Environ. Sci. Pollut. Res.* **2021**, *28*, 17275–17289. [[CrossRef](#)]
19. Marlon, J.R.; Bartlein, P.J.; Carcaillet, C.; Gavin, D.G.; Harrison, S.P.; Higuera, P.E.; Joos, F.; Power, M.J.; Prentice, I.C. Climate and Human Influences on Global Biomass Burning over the Past Two Millennia. *Nat. Geosci.* **2008**, *1*, 697–702. [[CrossRef](#)]
20. Earl, N.; Simmonds, I. Spatial and Temporal Variability and Trends in 2001–2016 Global Fire Activity. *J. Geophys. Res. Atmos.* **2018**, *123*, 2524–2536. [[CrossRef](#)]
21. Rogers, B.M.; Balch, J.K.; Goetz, S.J.; Lehmann, C.E.R.; Turetsky, M. Focus on Changing Fire Regimes: Interactions with Climate, Ecosystems, and Society. *Environ. Res. Lett.* **2020**, *15*, 030201. [[CrossRef](#)]
22. Sannigrahi, S.; Pilla, F.; Basu, B.; Basu, A.S.; Sarkar, K.; Chakraborti, S.; Joshi, P.K.; Zhang, Q.; Wang, Y.; Bhatt, S.; et al. Examining the Effects of Forest Fire on Terrestrial Carbon Emission and Ecosystem Production in India Using Remote Sensing Approaches. *Sci. Total Environ.* **2020**, *725*, 138331. [[CrossRef](#)]
23. Kochanski, A.K.; Jenkins, M.A.; Yedinak, K.; Mandel, J.; Beezley, J.; Lamb, B. Toward an Integrated System for Fire, Smoke and Air Quality Simulations. *Int. J. Wildland Fire* **2016**, *25*, 534. [[CrossRef](#)]
24. Zaehle, S.; Sitch, S.; Smith, B.; Hatterman, F. Effects of Parameter Uncertainties on the Modeling of Terrestrial Biosphere Dynamics. *Glob. Biogeochem. Cycles* **2005**, *19*, 1–16. [[CrossRef](#)]
25. Shi, Y.; Gong, S.; Zang, S.; Zhao, Y.; Wang, W.; Lv, Z.; Matsunaga, T.; Yamaguchi, Y.; Bai, Y. High-Resolution and Multi-Year Estimation of Emissions from Open Biomass Burning in Northeast China during 2001–2017. *J. Clean. Prod.* **2021**, *310*, 127496. [[CrossRef](#)]
26. Venkataraman, C.; Habib, G.; Kadamba, D.; Shrivastava, M.; Leon, J.-F.; Crouzille, B.; Boucher, O.; Streets, D.G. Emissions from Open Biomass Burning in India: Integrating the Inventory Approach with High-Resolution Moderate Resolution Imaging Spectroradiometer (MODIS) Active-Fire and Land Cover Data. *Global Biogeochem. Cycles* **2006**, *20*. [[CrossRef](#)]
27. Andreae, M.O.; Merlet, P. Emission of Trace Gases and Aerosols from Biomass Burning. *Global Biogeochem. Cycles* **2001**, *15*, 955–966. [[CrossRef](#)]
28. Avitabile, V.; Herold, M.; Heuvelink, G.B.M.; Lewis, S.L.; Phillips, O.L.; Asner, G.P.; Armston, J.; Ashton, P.S.; Banin, L.; Bayol, N.; et al. An Integrated Pan-tropical Biomass Map Using Multiple Reference Datasets. *Glob. Chang. Biol.* **2016**, *22*, 1406–1420. [[CrossRef](#)]
29. Kaufman, Y.J.; Justice, C.O.; Flynn, L.P.; Kendall, J.D.; Prins, E.M.; Giglio, L.; Ward, D.E.; Menzel, W.P.; Setzer, A.W. Potential Global Fire Monitoring from EOS-MODIS. *J. Geophys. Res. Atmos.* **1998**, *103*, 32215–32238. [[CrossRef](#)]
30. Wooster, M.J.; Roberts, G.; Freeborn, P.H.; Xu, W.; Govaerts, Y.; Beeby, R.; He, J.; Lattanzio, A.; Mullen, R. Meteosat SEVIRI Fire Radiative Power (FRP) Products from the Land Surface Analysis Satellite Applications Facility (LSA SAF)—Part 1: Algorithms, Product Contents and Analysis. *Atmos. Chem. Phys. Discuss.* **2015**, *15*, 15831–15907. [[CrossRef](#)]
31. Freeborn, P.H.; Wooster, M.J.; Hao, W.M.; Ryan, C.A.; Nordgren, B.L.; Baker, S.P.; Ichoku, C. Relationships between Energy Release, Fuel Mass Loss, and Trace Gas and Aerosol Emissions during Laboratory Biomass Fires. *J. Geophys. Res. Atmos.* **2008**, *113*, 1–17. [[CrossRef](#)]
32. Li, F.; Zhang, X.; Roy, D.P.; Kondragunta, S. Estimation of Biomass-Burning Emissions by Fusing the Fire Radiative Power Retrievals from Polar-Orbiting and Geostationary Satellites across the Conterminous United States. *Atmos. Environ.* **2019**, *211*, 274–287. [[CrossRef](#)]
33. Vermote, E.; Ellicott, E.; Dubovik, O.; Lapyonok, T.; Chin, M.; Giglio, L.; Roberts, G.J. An Approach to Estimate Global Biomass Burning Emissions of Organic and Black Carbon from MODIS Fire Radiative Power. *J. Geophys. Res. Atmos.* **2009**, *114*, D18205. [[CrossRef](#)]
34. Boschetti, L.; Roy, D.P. Strategies for the Fusion of Satellite Fire Radiative Power with Burned Area Data for Fire Radiative Energy Derivation. *J. Geophys. Res. Atmos.* **2009**, *114*, D20302. [[CrossRef](#)]

35. Zhang, X.; Kondragunta, S.; Schmidt, C.; Kogan, F. Near Real Time Monitoring of Biomass Burning Particulate Emissions (PM_{2.5}) across Contiguous United States Using Multiple Satellite Instruments. *Atmos. Environ.* **2008**, *42*, 6959–6972. [[CrossRef](#)]
36. Konovalov, I.B.; Lvova, D.A.; Beekmann, M.; Jethva, H.; Mikhailov, E.F.; Paris, J.-D.; Belan, B.D.; Kozlov, V.S.; Ciais, P.; Andreae, M.O. Estimation of Black Carbon Emissions from Siberian Fires Using Satellite Observations of Absorption and Extinction Optical Depths. *Atmos. Chem. Phys.* **2018**, *18*, 14889–14924. [[CrossRef](#)]
37. Bar, S.; Parida, B.R.; Roberts, G.; Pandey, A.C.; Acharya, P.; Dash, J. Spatio-Temporal Characterization of Landscape Fire in Relation to Anthropogenic Activity and Climatic Variability over the Western Himalaya, India. *GIScience Remote Sens.* **2021**, *58*, 281–299. [[CrossRef](#)]
38. Babu, K.V.S.; Roy, A.; Prasad, P.R. Forest Fire Risk Modeling in Uttarakhand Himalaya Using TERRA Satellite Datasets. *Eur. J. Remote Sens.* **2016**, *49*, 381–395. [[CrossRef](#)]
39. Prabhakar, R.; Somanathan, E.; Mehta, B.S. How Degraded Are Himalayan Forests? *Curr. Sci.* **2006**, *91*, 61–67.
40. Murmu, M.; Roy, A.; Karnatak, H.C.; Chauhan, P. Impact Of Forest Fire Emissions On Air Quality Over Western Himalaya Region. *Int. Arch. Photogramm. Remote Sens. Spat. Inf. Sci.* **2022**, *XLIII-B3-2*, 1153–1160. [[CrossRef](#)]
41. Yarragunta, Y.; Srivastava, S.; Mitra, D.; Chandola, H.C. Influence of Forest Fire Episodes on the Distribution of Gaseous Air Pollutants over Uttarakhand, India. *GIScience Remote Sens.* **2020**, *57*, 190–206. [[CrossRef](#)]
42. Negi, P.S.; Pandey, C.P.; Singh, N. Black Carbon Aerosols in the Ambient Air of Gangotri Glacier Valley of North-Western Himalaya in India. *Atmos. Environ.* **2019**, *214*, 116879. [[CrossRef](#)]
43. Negi, P.S.; Pandey, C.P. Black Carbon Pollutants in Pristine Himalayan Ecosystem: A Pilot Study along Gangotri Glacier Valley. *Environ. Monit. Assess.* **2021**, *193*, 726. [[CrossRef](#)] [[PubMed](#)]
44. Prabhu, V.; Soni, A.; Madhwal, S.; Gupta, A.; Sundriyal, S.; Shridhar, V.; Sreekanth, V.; Mahapatra, P.S. Black Carbon and Biomass Burning Associated High Pollution Episodes Observed at Doon Valley in the Foothills of the Himalayas. *Atmos. Res.* **2020**, *243*, 105001. [[CrossRef](#)]
45. Gul, C.; Mahapatra, P.S.; Kang, S.; Singh, P.K.; Wu, X.; He, C.; Kumar, R.; Rai, M.; Xu, Y.; Puppala, S.P. Black Carbon Concentration in the Central Himalayas: Impact on Glacier Melt and Potential Source Contribution. *Environ. Pollut.* **2021**, *275*, 116544. [[CrossRef](#)]
46. Yasunari, T.J.; Tan, Q.; Lau, K.-M.; Bonasoni, P.; Marinoni, A.; Laj, P.; Ménégoz, M.; Takemura, T.; Chin, M. Estimated Range of Black Carbon Dry Deposition and the Related Snow Albedo Reduction over Himalayan Glaciers during Dry Pre-Monsoon Periods. *Atmos. Environ.* **2013**, *78*, 259–267. [[CrossRef](#)]
47. Kumar, R.; Naja, M.; Satheesh, S.K.; Ojha, N.; Joshi, H.; Sarangi, T.; Pant, P.; Dumka, U.C.; Hegde, P.; Venkataramani, S. Influences of the Springtime Northern Indian Biomass Burning over the Central Himalayas. *J. Geophys. Res. Atmos.* **2011**, *116*, D19302. [[CrossRef](#)]
48. Bali, K.; Mishra, A.K.; Singh, S. Impact of Anomalous Forest Fire on Aerosol Radiative Forcing and Snow Cover over Himalayan Region. *Atmos. Environ.* **2017**, *150*, 264–275. [[CrossRef](#)]
49. Giglio, L.; Boschetti, L.; Roy, D.P.; Humber, M.L.; Justice, C.O. The Collection 6 MODIS Burned Area Mapping Algorithm and Product. *Remote Sens. Environ.* **2018**, *217*, 72–85. [[CrossRef](#)] [[PubMed](#)]
50. Bar, S.; Parida, B.R.; Shankar, B.U. Unfolding the Contribution of Environmental and Anthropogenic Variables in Forest Fire over Western Himalayan Fire Regime. In Proceedings of the 2021 IEEE International India Geoscience and Remote Sensing Symposium (InGARSS), Ahmedabad, India, 6–10 December 2021; pp. 557–560.
51. Bar, S.; Parida, B.R.; Pandey, A.C. Landsat-8 and Sentinel-2 Based Forest Fire Burn Area Mapping Using Machine Learning Algorithms on GEE Cloud Platform over Uttarakhand, Western Himalaya. *Remote Sens. Appl. Soc. Environ.* **2020**, *18*, 100324. [[CrossRef](#)]
52. Roteta, E.; Bastarrika, A.; Padilla, M.; Storm, T.; Chuvieco, E. Development of a Sentinel-2 Burned Area Algorithm: Generation of a Small Fire Database for Sub-Saharan Africa. *Remote Sens. Environ.* **2019**, *222*, 1–17. [[CrossRef](#)]
53. Shi, Y.; Matsunaga, T.; Saito, M.; Yamaguchi, Y.; Chen, X. Comparison of Global Inventories of CO₂ Emissions from Biomass Burning during 2002–2011 Derived from Multiple Satellite Products. *Environ. Pollut.* **2015**, *206*, 479–487. [[CrossRef](#)]
54. Akagi, S.K.; Yokelson, R.J.; Wiedinmyer, C.; Alvarado, M.J.; Reid, J.S.; Karl, T.; Crounse, J.D.; Wennberg, P.O. Emission Factors for Open and Domestic Biomass Burning for Use in Atmospheric Models. *Atmos. Chem. Phys.* **2011**, *11*, 4039–4072. [[CrossRef](#)]
55. McMeeking, G.R. The Optical, Chemical, and Physical Properties of Aerosols and Gases Emitted by the Laboratory Combustion of Wildland Fuels; Dissertation Abstracts International. Ph.D. Thesis, Colorado State University, Fort Collins, CO, USA, 2008.
56. Randerson, J.T.; Van Der Werf, G.R.; Giglio, L.; Collatz, G.J.; Kasibhatla, P.S. *Global Fire Emissions Database, Version 4.1 (GFEDv4)*; ORNL DAAC: Oak Ridge, TN, USA, 2015. [[CrossRef](#)]
57. Sulla-Menashe, D.; Friedl, M. MCD12Q1 MODIS/Terra+Aqua Land Cover Type Yearly L3 Global 500m SIN Grid V006. *NASA EOSDIS L. Process. DAAC* **2015**, *10*, 200. [[CrossRef](#)]
58. Giglio, L.; Randerson, J.T.; van der Werf, G.R. Analysis of Daily, Monthly, and Annual Burned Area Using the Fourth-Generation Global Fire Emissions Database (GFED4). *J. Geophys. Res. Biogeosci.* **2013**, *118*, 317–328. [[CrossRef](#)]
59. Randerson, J.T.; Chen, Y.; van der Werf, G.R.; Rogers, B.M.; Morton, D.C. Global Burned Area and Biomass Burning Emissions from Small Fires. *J. Geophys. Res. Biogeosci.* **2012**, *117*. [[CrossRef](#)]
60. Saatchi, S.S.; Harris, N.L.; Brown, S.; Lefsky, M.; Mitchard, E.T.A.; Salas, W.; Zutta, B.R.; Buermann, W.; Lewis, S.L.; Hagen, S.; et al. Benchmark Map of Forest Carbon Stocks in Tropical Regions across Three Continents. *Proc. Natl. Acad. Sci. USA* **2011**, *108*, 9899–9904. [[CrossRef](#)] [[PubMed](#)]

61. Baccini, A.; Goetz, S.J.; Walker, W.S.; Laporte, N.T.; Sun, M.; Sulla-Menashe, D.; Hackler, J.; Beck, P.S.A.; Dubayah, R.; Friedl, M.A.; et al. Estimated Carbon Dioxide Emissions from Tropical Deforestation Improved by Carbon-Density Maps. *Nat. Clim. Chang.* **2012**, *2*, 182–185. [[CrossRef](#)]
62. Santoro, M.; Beaudoin, A.; Beer, C.; Cartus, O.; Fransson, J.E.S.; Hall, R.J.; Pathe, C.; Schmillius, C.; Schepaschenko, D.; Shvidenko, A.; et al. Forest Growing Stock Volume of the Northern Hemisphere: Spatially Explicit Estimates for 2010 Derived from Envisat ASAR. *Remote Sens. Environ.* **2015**, *168*, 316–334. [[CrossRef](#)]
63. Santoro, M.; Beer, C.; Cartus, O.; Schmillius, C.; Shvidenko, A.; McCallum, I.; Wegmüller, U.; Wiesmann, A. Retrieval of Growing Stock Volume in Boreal Forest Using Hyper-Temporal Series of Envisat ASAR ScanSAR Backscatter Measurements. *Remote Sens. Environ.* **2011**, *115*, 490–507. [[CrossRef](#)]
64. Huete, A.; Justice, C.; Van Leeuwen, W. MODIS Vegetation Index (MOD13). *Algorithm Theor. basis Doc.* **1999**, *3*, 295–309.
65. Justice, C.O.; Vermote, E.; Townshend, J.R.G.; Defries, R.; Roy, D.P.; Hall, D.K.; Salomonson, V.V.; Privette, J.L.; Riggs, G.; Strahler, A. The Moderate Resolution Imaging Spectroradiometer (MODIS): Land Remote Sensing for Global Change Research. *IEEE Trans. Geosci. Remote Sens.* **1998**, *36*, 1228–1249. [[CrossRef](#)]
66. Van Der Werf, G.R.; Randerson, J.T.; Giglio, L.; Collatz, G.J.; Mu, M.; Kasibhatla, P.S.; Morton, D.C.; Defries, R.S.; Jin, Y.; Van Leeuwen, T.T. Global Fire Emissions and the Contribution of Deforestation, Savanna, Forest, Agricultural, and Peat Fires (1997–2009). *Atmos. Chem. Phys.* **2010**. [[CrossRef](#)]
67. Wiedinmyer, C.; Quayle, B.; Geron, C.; Belote, A.; McKenzie, D.; Zhang, X.; O'Neill, S.; Wynne, K.K. Estimating Emissions from Fires in North America for Air Quality Modeling. *Atmos. Environ.* **2006**, *40*, 3419–3432. [[CrossRef](#)]
68. Wu, J.; Kong, S.; Wu, F.; Cheng, Y.; Zheng, S.; Yan, Q.; Zheng, H.; Yang, G.; Zheng, M.; Liu, D.; et al. Estimating the Open Biomass Burning Emissions in Central and Eastern China from 2003 to 2015 Based on Satellite Observation. *Atmos. Chem. Phys.* **2018**, *18*, 11623–11646. [[CrossRef](#)]
69. Bray, C.D.; Battye, W.; Aneja, V.P.; Tong, D.Q.; Lee, P.; Tang, Y. Ammonia Emissions from Biomass Burning in the Continental United States. *Atmos. Environ.* **2018**, *187*, 50–61. [[CrossRef](#)]
70. Ito, A.; Penner, J.E. Global Estimates of Biomass Burning Emissions Based on Satellite Imagery for the Year 2000. *J. Geophys. Res. Atmos.* **2004**, *109*, D14S05. [[CrossRef](#)]
71. Hansen, M.C.; Defries, R.S.; Townshend, J.R.G.; Sohlberg, R. Global Land Cover Classification at 1 Km Spatial Resolution Using a Classification Tree Approach. *Int. J. Remote Sens.* **2000**, *21*, 1331–1364. [[CrossRef](#)]
72. Shi, Y.; Zang, S.; Matsunaga, T.; Yamaguchi, Y. A Multi-Year and High-Resolution Inventory of Biomass Burning Emissions in Tropical Continents from 2001–2017 Based on Satellite Observations. *J. Clean. Prod.* **2020**, *270*, 122511. [[CrossRef](#)]
73. Anderson, G.K.; Sandberg, D.V.; Norheim, R.A. Fire Emission Production Simulator (FEPS) User's Guide. 2004. Available online: https://www.fs.fed.us/pnw/fera/publications/fulltext/FEPS_User_Guide.pdf (accessed on 22 June 2022).
74. Randerson, J.T.; Van Der Werf, G.R.; Giglio, L.; Collatz, G.J.; Kasibhatla, P.S. *Global Fire Emissions Database, Version 4, (GFEDv4)*; ORNL DAAC: Oak Ridge, TN, USA, 2018. [[CrossRef](#)]
75. Rolph, G.; Stein, A.; Stunder, B. Real-Time Environmental Applications and Display System: READY. *Environ. Model. Softw.* **2017**, *95*, 210–228. [[CrossRef](#)]
76. Haridas, M.K.M.; Rao, P.V.N.; Rao, K.S.; Sudhakar, P. Studies of Forest Fire Induced Changes in Atmosphere over Uttarakhand, India, Using Space Based Observations and Model Simulations. *Curr. Sci.* **2018**, *114*, 2504–2512. [[CrossRef](#)]
77. Reddy, C.S.; Bird, N.G.; Sreelakshmi, S.; Manikandan, T.M.; Asra, M.; Krishna, P.H.; Jha, C.S.; Rao, P.V.N.; Diwakar, P.G. Identification and Characterization of Spatio-Temporal Hotspots of Forest Fires in South Asia. *Environ. Monit. Assess.* **2019**, *191*, 791. [[CrossRef](#)]
78. Kumar, A.; Bali, K.; Singh, S.; Naja, M.; Mishra, A.K. Estimates of Reactive Trace Gases (NMVOCs, CO and NO_x) and Their Ozone Forming Potentials during Forest Fire over Southern Himalayan Region. *Atmos. Res.* **2019**, *227*, 41–51. [[CrossRef](#)]
79. Gong, P.; Wang, X. Forest Fires Enhance the Emission and Transport of Persistent Organic Pollutants and Polycyclic Aromatic Hydrocarbons from the Central Himalaya to the Tibetan Plateau. *Environ. Sci. Technol. Lett.* **2021**, *8*, 498–503. [[CrossRef](#)]
80. Chatterjee, A.; Mukherjee, S.; Dutta, M.; Ghosh, A.; Ghosh, S.K.; Roy, A. High Rise in Carbonaceous Aerosols under Very Low Anthropogenic Emissions over Eastern Himalaya, India: Impact of Lockdown for COVID-19 Outbreak. *Atmos. Environ.* **2021**, *244*, 117947. [[CrossRef](#)] [[PubMed](#)]
81. Sandeep, K.; Panicker, A.S.; Gautam, A.S.; Beig, G.; Gandhi, N.; S, S.; Shankar, R.; Nainwal, H.C. Black Carbon over a High Altitude Central Himalayan Glacier: Variability, Transport, and Radiative Impacts. *Environ. Res.* **2022**, *204*, 112017. [[CrossRef](#)]
82. Shi, Y.; Matsunaga, T.; Yamaguchi, Y. High-Resolution Mapping of Biomass Burning Emissions in Three Tropical Regions. *Environ. Sci. Technol.* **2015**, *49*, 10806–10814. [[CrossRef](#)]